Texture and interface characterization of iridium thin films grown on MgO substrates with different orientations

Lucian Trupina, Liviu Nedelcu, Marian Gabriel Banciu, Aurelian Crunteanu, Laure Huitema, Catalin Constantinescu, Alexandre Boulle

Texture and interface characterization of iridium thin films grown on MgO substrates with different orientations

[1]*Lucian TRUPINA*[1], *Liviu NEDELCU*[1], *Marian Gabriel BANCIU*[1],
Aurelian CRUNTEANU[2], *Laure HUITEMA*[2], [*]*Cătălin CONSTANTINESCU*[3], *Alexandre BOULLE*[3]

[1] *National Institute of Materials Physics,*
Bd. Atomistilor 405A, RO-077125 Magurele, Romania

[2] *XLIM - UMR 7252, CNRS, University of Limoges,*
123 av. Albert Thomas, F-87060 Limoges, France

[3] *IRCER - UMR 7315, CNRS, University of Limoges,*
12 rue Atlantis, F-87068 Limoges, France

Abstract

Iridium thin films are grown by direct-current plasma magnetron sputtering, on MgO single crystal substrates with various surface orientation, *i.e.* (100), (111) and (110). The surface morphology, the crystalline properties of the films, and the substrate - thin film interface, are investigated by atomic force microscopy (AFM), X-ray diffraction (XRD), focused ion beam scanning electron microscopy (FIB-SEM), and high-resolution transmission electron microscopy (HR-TEM), respectively. The results reveal that hetero-epitaxial thin films with different crystallographic orientation and notable atomic scale smooth surface are obtained. From the XRD analysis the following epitaxial relations are obtained: *i)* $(100)_{Ir}$ || $(100)_{MgO}$ out-of-plane and $[001]_{Ir}$ || $[001]_{MgO}$ in-plane for Ir grown on MgO(100), *ii*) $(110)_{Ir}$ || $(110)_{MgO}$ out-of-plane and $[1\text{-}10]_{Ir}$ || $[1\text{-}10]_{MgO}$ in-plane for Ir grown on MgO(110) and *iii*) $(111)_{Ir}$ || $(111)_{MgO}$ out-of-plane and two variants for in-plane orientation $[1\text{-}10]_{Ir}$ || $[1\text{-}10]_{MgO}$ and $[1\text{-}10]_{Ir}$ || $[10\text{-}1]_{MgO}$, respectively for Ir grown on MgO(111). Because of the large misfit strain (9.7%), the thin films are found to grow in a strain-relaxed state with the formation of geometrical misfit dislocations with a ~2.8 nm spacing, whereas thermal strain is stored upon cooling down from the growth temperature (600 °C). The best structural characteristics are obtained for the (111) oriented films with a mosaicity of 0.3° and vanishingly small lattice distortions. The (100)- and (110)-oriented films exhibit mosaicities of ~1.2° and lattice distortions of ~1% which can be explained by the larger surface energy of these planes as compared to (111).

Keywords: *iridium, thin film, epitaxy, texturation, interface, lattice distortion, mosaicity.*

1. Introduction

The crystallographic orientation of a metal thin film affects its surface energy and structure. Surface chemical reactions and interface engineering, which are important in applications including optoelectronic devices and catalysis, as well as understanding crystalline growth, are therefore of paramount importance [1-5]. In this respect, iridium layers that are crystallographically oriented, exhibit low stress, yet high density and low surface roughness, find widespread use in various high-end technological applications, such

[1] Electronic mail: *lucian.trupina@infim.ro*, *catalin.constantinescu@unilim.fr*

as diffusion barrier material in ferroelectric random access memories, gate electrode in field effect transistors, template layer for diamond hetero-epitaxy, active layers in gas sensors, hydrogen separation membranes or materials for electro-catalyst [6-9], and even in ultra-high quality grazing incidence configuration mirror elements of the Advanced X-ray Astrophysics Facility – Imaging (AXAF–I), a space-based X-ray observatory of NASA [10, 11]. The lattice parameter of iridium is 0.38386 nm at 270 K [12, 13]. The surface morphology and the crystallographic orientation of such thin films have a significant influence on their electrical and optical properties, as well as the rate of chemical reactions at the film surface, and hence on the foreseen applications. Growth of thin films with high-energy surface are extremely important especially in catalysts, because such surfaces exhibit a high density of active sites [14, 15]. Chemisorption can lead to not only the restructuring of adsorbates but also a significant reconstruction of single crystal surfaces [16, 17]. In many cases, massive reconstruction on clean surfaces can lead to a surface structure totally different from that projected from bulk structure. This is the case for reconstructed Ir(100) or Ir(110) surfaces [18, 19]. The dissociative chemisorption of O_2 and the properties of chemisorbed oxygen atoms on Ir(111) have also been studied in detail and are generally well understood [20]. These effects are very important in applications such as thin films and multi-layered structures [21], *e.g*. in metal-insulator-metal (MIM) capacitive applications [22]. The use of iridium as bottom electrode in MIM-type devices was also found to influence the preferred orientation and microstructure, as well as the surface morphology, of para-/ferro-electric films grown on Ir [21-25].

Single crystal MgO with various crystallographic cuts is commonly used as a substrate for the deposition of a wide range of thin film materials, in many different areas of research such as superconductors, and other types of oxides, metal and nitride films, multilayers and superlattices. In particular, highly lattice-mismatched metals with a controlled orientation can be developed, since the substrate lattice acts as a template for growth [1-3, 22, 26-28]. Growth of hetero-epitaxial (100) iridium thin films on (100) MgO single crystal [28] or on MgO-buffered Si(100) [29] substrate has been reported by pulsed laser deposition (PLD) and radiofrequency (RF)-powered plasma magnetron sputtering, while (111) oriented iridium films have been obtained by electron-beam evaporation (EBE) on yttria-stabilized zirconia-buffered silicon substrate [30] or by direct-current (DC) magnetron sputtering technique on TiO_2 buffered silicon substrate [31].

In this study, we present and discuss results on the growth of hetero-epitaxial iridium thin films with (100), (111), and (110) crystallographic orientations, respectively, grown on single crystal MgO substrates with the corresponding crystallographic orientation. A comparison of the crystalline properties and the morphology of the films is performed. For all three orientations, the level of residual strain, the interface structures and the overall structural quality are discussed with regard to growth mechanism and the surface energies of the corresponding orientations.

2. Experimental

The Ir thin films have been fabricated by DC-magnetron sputtering using a pure (99.9%) iridium target in a Gamma 1000C sputtering system with a base pressure of ~3 x 10^{-5} Pa. The chosen substrates, *i.e.* single side polished MgO (100), (110) and (111) oriented single crystals (flux melt crystal growth, 10 x 10 mm square samples, 500 µm in thickness, one side polished, R_q <1.0 nm), have been heat-treated at 1050 °C for 5 hours in air and at atmospheric pressure. This procedure has proven effective in obtaining clean MgO surfaces with regular atomic step-and-terrace structures. The thin films have been deposited at 600 °C substrate temperature and 0.66 Pa, in argon atmosphere. The applied density power on the iridium target was 1 W/cm², corresponding to a deposition rate of ~0.5 nm/min. Various thin film thicknesses have been obtained. Further details on the deposition procedure are presented elsewhere [31]. The epitaxial relationships and the microstructural properties of the films (thickness, roughness, lattice distortions and lattice strain) have been investigated using X-ray diffraction (XRD). All measurements have been performed on a Bruker D8 Discover diffractometer, equipped with Cu target (λ = 1.5406 Å), and a parabolic mirror associated with a two-reflection Ge monochromator. Diffracted X-rays are collected using a 1D (LynxEye) detector covering a 2° 2θ range with an angular resolution of 0.01°. The film lattice parameters and residual strains have been determined by the analysis of reciprocal space maps (RSMs) of reflections with *hkl* indices containing both in-plane and out-of-plane components (*i.e.* asymmetrical RSMs). The surface morphology and roughness of the films have been investigated by atomic force microscopy (AFM), by using a MFP 3D SA microscope. Scanning electron microscopy (SEM) surface investigations, cross-section thickness measurements, and further sample processing, have been performed on a ZEISS Crossbeam 550 focused ion beam scanning electron microscope (FIB-SEM) equipped with a

nanomanipulator for 3D analytics and sample preparation. This device was used in preparing transmission electron microscopy (TEM) samples, by using the low voltage capabilities of the FIB ion-sculptor to get ultra-thin samples while keeping amorphization damage at a minimum. Finally, the high-resolution (HR) TEM investigations of the iridium films and MgO substrates / thin films interfacial properties have been assessed on a Jeol JEM-2100F, 200 kV FE (field emission) analytical electron microscope.

3. Results and discussion

The growth of (100) or (110)-oriented iridium thin films is challenging because the {111} close packed planes have the lowest surface free energy of 2.59 J/m², followed by the {100} planes with 2.95 J/m², and by the {110} planes with 3.19 J/m² [32]. For this reason, the (111) crystalline orientation is preferred when the growth is governed by the low surface energy of the film. For instance, in the case of iridium films grown on silicon substrates under various deposition conditions, a preferential (111)-orientation has been systematically observed [31]. However, changing the nature and the structure of the substrate might yield to favourable interface energies, allowing the epitaxial growth of different orientations, as it is observed in the present work.

As previously stated, at room temperature iridium has a face centred cubic (*fcc*) structure with a unit cell edge length of 0.38386 nm. MgO substrate has a *fcc*-type lattice of Mg ions with O ions occupying all the octahedral sites (and vice versa) with a unit cell edge length of 0.4211 nm. The possible hetero-epitaxial relations between iridium films and MgO (001), (111) and (110) substrates are schematically shown in *Figure 1*. The substrate-film misfit strain is defined as:

$$e = \frac{a_s - a_f}{a_f},$$

where $a_{(s/f)}$ represent the lattice constants of the substrate and the film. Since the film and the substrate exhibit the same orientations regardless of the substrates cut, the misfit strain is constant for all films and equals 9.7% (tensile). In the case of large lattice mismatch, hetero-epitaxial growth is possible via rotation domains hetero-epitaxy or domain matching hetero-epitaxy, and the associated formation of “geometrical” misfit dislocations [1-3, 33, 34]. The adjective “geometrical” is here used to indicate that these dislocations are directly formed at the interface during growth and do not require the glide of dislocations from the

surface, as it is usually the case for lower lattice mismatch [35]. Interestingly, this potentially leads to high quality films to due to the lack of threading dislocation segments. The dislocation spacing is given by *b/e* (with "*b*" being the magnitude of the Burgers vector of the dislocations) which, with the above strain value, gives an average of 2.8 nm. This value has been obtained assuming the Burgers vector b = ½<110>, which, in the case of *fcc* metals, corresponds to perfect dislocations with the lowest energy. The XRD characterizations corresponding to iridium films grown onto MgO(100), MgO(110) and MgO(111) substrates are given in *Figure 2*, *Figure 3* and *Figure 4*, respectively. Let us first discuss the case of MgO(100) in detail.

In *Figure 2a*, only the *h00* reflections of iridium are visible, together with the *h00* reflections of MgO, which indicates the (100) planes of iridium are parallel to the (100) planes of MgO. In this data, as well as in the following θ-2θ scans, additional peaks, labelled "*", are visible. Those peaks actually correspond to a residual of K_β radiation. Although a two-reflection monochromator is used, a fraction of this radiation escapes the monochromator. Such radiations are usually cut out using a slit at the output of the monochromator, which was not the case for these experiments. However, this has no consequences on the results presented below. The in-plane orientation has been determined by φ-scan measurement using the (420) reflection plane of both MgO and iridium, as presented in *Figure 2b*. The reflections occur at the same azimuthal angle which demonstrates that the [010] direction of iridium is parallel to the [010] of MgO. The four symmetric peaks of the φ-scan indicate that the iridium film is grown cube-on-cube, with epitaxial relationship to MgO(100), exhibiting the $(100)_{Ir}$ || $(100)_{MgO}$ out-of-plane orientation and $[001]_{Ir}$ || $[001]_{MgO}$ in-plane orientation. The inset in *Figure 2a* shows the simulation of the 200 reflection of iridium with a thin film scattering model from which were calculated the film thickness *t*, the roughness *r* (root-mean-squared (RMS) thickness fluctuations, $\langle (t - \langle t \rangle)^2 \rangle^{1/2}$), and the lattice distortions *ε* (RMS lattice plane distortions, $\langle d - \langle d \rangle)^2 \rangle^{1/2} / d$). The obtained values are *t* = 23.2 nm, *r* = 0.7 nm, and *ε* = 0.012, respectively. Details regarding the scattering model can be found in reference [36], equation (5). Further information regarding thin film quality can be obtained from the rocking curves recorded through the *h00* reflections of iridium, presented in *Figure 2c*. The rocking curves have been simulated with a Pearson VII function; the full-width at half-maximum (FWHM) gives the mosaicity, which is 1.26 and 1.22° for the 200 and 400, respectively. Finally, the state of strain of the film was

obtained from the analysis of 311 RSMs. Such a RSM is shown in *Figure 2d*. Knowing the films orientation and the elastic constants of iridium, it is possible to compute the state of strain, $e_{//}$, as well as the bulk (strain-free) lattice parameter, $a^{(bulk)}$, of the film from the coordinates of the reflections of iridium and MgO. For this purpose, we follow the approach detailed in reference [37], where $a^{(bulk)}$ and $e_{//}$ can be deduced from the in-plane, $d_{//} = 2\pi/Q_{//}$, and out-of-plane, $d_{\perp} = 2\pi/Q_{\perp}$, lattice spacing determined from the RSM:

$$d_{//}^{(bulk)} = \frac{d_{\perp} + d_{//}\nu_2 tan\phi}{(1+\nu_2)tan\phi}$$

In the case of the (100) orientation and the 311 reflection, $Q_{//} = Q_{[011]}$, $Q_{\perp} = Q_{[100]}$, Φ is the angle between the (100) and the (311) planes and $d_{//}^{(bulk)} = a^{(bulk)} / 2^{1/2}$. For a (100) oriented film, the bi-axial Poisson ratio, υ_2, is given in *Table 1*. The peak coordinates ($Q_{//}$ and $Q_{\perp}$) have been obtained by fitting the RSM with 2-dimensional Gaussian functions using the *DxTools* program [38]. The in-plane strain, $e// = [d// - d//^{(bulk)}]/d//^{(bulk)}$, is found to be compressive, with e// = -0.353(9)%. Although the theoretical misfit strain is tensile (9.7%), this apparent discrepancy can be explained by the fact that such a high misfit strain cannot be sustained by the film which therefore grows in a strain-relaxed state (with, as mentioned earlier, the formation of geometrical misfit dislocations with a spacing of ~2.8 nm in the present case). Strain is subsequently stored upon cooling down from the growth temperature. Since the coefficient of thermal expansion (CTE) of magnesium oxide, *i.e.* ~12.6 x 10^{-6} K^{-1} in the RT-700 °C range [39], is higher that the CTE of iridium, *i.e.* ~7.29 x 10^{-6} K^{-1} in the RT-700 °C range [13], this gives rise to a theoretical compressive strain of $e = (\alpha_f - \alpha_s)(T_{growth} - RT) = -0.31\%$. This value is in good agreement with the value of $e_{//}$ determined above. As shown below, a similar value is found for all films. Finally, it is worth considering the strain-free lattice parameter. Surprisingly, $a^{(bulk)}$ is not equal to the theoretical value of iridium, but it exhibits a -3.58% shrinkage, *i.e.* 3.8254 Å instead of 3.8392 Å. This might indicate the presence of iridium vacancies introduced during growth. A similar value is found for the (111) oriented films which seems to indicate that this is a process-dependent phenomenon. A reliable value could not be determined for the (110) orientation because of the mosaic nature of this particular MgO substrate (see discussion below).

The same procedure has been used in the case of iridium grown on MgO(111) substrate. All numerical results are also presented in *Table 1*. From the θ-2θ and φ-scans shown in *Figure 3a* and *Figure 3b*, the following epitaxial relations are obtained: *i*) out-of-

plane: $(111)_{Ir}$ || $(111)_{MgO}$, *ii*) in-plane variant 1: $[1\text{-}10]_{Ir}$ || $[1\text{-}10]_{MgO}$ (180 and ± 60°) and variant 2: $[1\text{-}10]_{Ir}$ || $[10\text{-}1]_{MgO}$ (0 and ± 120°). The existence of two epitaxial variants comes from the fact that there are two possibilities (related by a 180° rotation) to position the iridium unit-cell on the MgO unit-cell: the iridium triangle points either "upwards", or "downwards", as one may conclude from the schematic in *Figure 1b*. From a structural point of view, variant 1 preserves the *fcc* ABC|ABC stacking across the interface (the interface being represented with the "|"), whereas variant 2 corresponds to: ABC|BCA, *i.e.* a stacking fault is formed at the interface. The energetic cost associated with the stacking fault probably explains why variant 2 is less likely to occur (~100× weaker intensity in the φ-scan).

Hetero-epitaxial iridium thin films have also been achieved on MgO(110) substrates, although it was more difficult to determine the state of strain and the unit-cell shrinkage do to the poor quality of the MgO crystals. It should be noted that this is a fairly general characteristic of MgO single crystals which are often "multi-crystalline" (or twinned) instead of purely single-crystalline. Indeed, more than 70% of the MgO substrates from six different vendors that have been tested for "single crystal" characteristics by Schroeder *et al* were demonstrated to be of less than the claimed single crystal quality [40]. Here, in the case of the (100)- and (111)- oriented ones, it was experimentally possible to select regions of the MgO crystals where the amounts of twins were low enough to perform a reliable characterization. Unfortunately, regions of sufficiently high quality could not be found for the (110)-oriented crystals. Nonetheless, from the θ-2θ scan, only (220) reflection peaks appear for both iridium and MgO, which corresponds to the $(110)_{Ir}$ || $(110)_{MgO}$ out-of-plane orientation. Φ-scans results on the (400) reflections of iridium reveal that the film had a $[1\text{-}10]_{Ir}$ || $[1\text{-}10]_{MgO}$ in-plane crystalline orientation with a twofold symmetry indicated by the peak separation of 180°, as presented in *Figure 4*.

As mentioned earlier, it is noteworthy that, within experimental uncertainty, all films exhibit the same level of strain, which can be solely explained by the CTE mismatch between iridium and MgO. Interestingly, although the (111)-oriented iridium thin film has a thickness 3 times larger than the other orientations, this does not seem to induce any strain relaxation. Therefore, this leads us to conclude that the differences in the structural characteristics between the different films cannot be attributed to interfacial strain, but solely to the interface energy of the different orientations. Being the lowest energy orientation, the (111)-oriented films exhibit the best structural quality with a mosaicity 4

times lower than (100) and (110), and a vanishingly small level of lattice distortions. On the other hand, the surface energies of the (100) and (110) orientation are similar which leads to similar mosaicities and distortions, namely 1.26° and 0.012, and 1.3° and 0.011, respectively.

The AFM investigations, as presented in *Figure 5*, as well as the SEM analysis of the iridium thin films (not presented here), show that not only the crystalline orientation of iridium thin films depends on the crystalline orientation of MgO substrate but also their surface morphology. Hetero-epitaxial growth and morphology of iridium thin films are directly influenced by surface step-terraces periodicity, corner sites and other substrate surface defects which may act as nucleation sites. The surface morphology of iridium thin films grown on MgO(001) substrates has a homogenous microstructure represented by rectangular grain shape arranged regularly and compactly with a RMS surface roughness of approximately 5.8 Å, as presented in *Figure 5a*. In case of the Ir(111) thin films grown on MgO(111) substrates, the surface morphology shows formations of triangular pyramidal-shaped grains. This reflects strong (111) orientation of *fcc* iridium structure and a surface roughness of approximately 8.5 Å, as presented in *Figure 5b*. Elongated rectangular grain shapes oriented along the same direction with lateral dimensions close to the width of the substrate terraces have been observed on Ir(110) grown on MgO(110), as shown by the AFM image presented in *Figure 5c*. The Ir(110) film exhibits a roughness of approximately 7.4 Å. It can be noted that, although different, these roughness values are of the same order of magnitude as those derived by XRD, i.e. 6.8 Å, 3.8 Å and 10 Å. The differences are most likely due to the fact that the AFM determination is local (with only a few μm^2 probed), whereas XRD probes several mm^2.

In order to assess the quality and structure of the iridium thin films and the corresponding MgO substrates, TEM sample slides (~20 × 7 µm) are cut by FIB and then soldered to the TEM holders with Pt, as shown in *Supplementary Material*. Samples are finally refined and thinned by FIB and with the help of a nanomanipulator are further transported and investigated. HR-TEM investigations of the iridium thin films *vs.* MgO substrates have been acquired at different magnifications and in several zones for all three crystalline orientations. Selected area electron diffraction (SAED) patterns have been recorded on the iridium thin film, the substrate, as well as on the substrate – thin film interfacial region for all samples, as shown in *Supplementary Material* (electron beam with a 1 nm diameter, at 200 kV acceleration voltage). Unsurprisingly, these measurements

correspond to the epitaxial orientation determined by XRD. In *Figure 6a*, the HR-TEM image of Ir(001) grown on MgO-(001) is presented. One may observe the crystallographic orientation and the neat interfacial continuity between the substrate and the thin film. Although some dislocations can be observed at the film/substrate interface, it is important to note that the film is almost defect free, in particular no threading segments of dislocations are to be observed. This observation is in good agreement with the above-mentioned domain-matching growth mechanism. In order to enhance the contrast of the interface misfit, a digital dark-field image of the interface has been generated by selecting the 002 and 00-2 reflections in the Fourier transformed image. The corresponding filtered image is displayed in *Figure 6b*. It can be noted that the in-plane lattice spacing can be computed from the plane period (far from the distorted region at the interface), which yields d_{200} = 1.915 Å, *i.e.* a = 2×d_{200} = 3.83 Å (in very good agreement with the strain-free lattice parameter obtained by XRD, 3.8254 Å). In this image, the geometrical misfit dislocations are now clearly observed (red circles), from which the dislocation spacing can be computed. Before proceeding, it should be emphasized that, since the Burger vector of the dislocation is of ½<110> type, with the (001) film orientation, two sets of dislocations are actually formed at the interface with Burgers vector ½[011] and ½[011], and dislocations lines extending along [011] and [011], respectively. Since the TEM image has been taken along the [010] zone axis, the apparent dislocation spacing is increased by a factor of $2^{½}$. However, since both sets of dislocations contribute to the image, the overall dislocation density is actually overestimated by a factor of $2^{½}$. With 18 visible dislocations, the average spacing, corrected for the above-mentioned $2^{½}$ factor, is 2.94 nm, in relatively good agreement with the value expected from the domain-matching interface model (2.8 nm). *Figure 7a* and *Figure 7b* show the same images for the (111) orientation. Unfortunately, the quality of the sample preparation here is not sufficient to get a highly resolved image, so that even the Fourier filtered image is difficult to interpret. Nonetheless, by compressing the image along the selected {00l} planes (*Figure 7c*) it is possible to resolve some misfit dislocations. Six dislocations can be distinguished with a computed spacing of 2.91 nm. Finally, the (110) orientation is depicted in *Figure 8*. The most striking feature is the peculiar morphology of the MgO surface which exhibits trenches perpendicular to the zone axis. Although the origin of those trenches is not yet determined, it might be due to a roughening transition occurring during the heat treatment to which the MgO substrates are submitted before deposition.

Despite these substrate surface features, one may observe that the iridium thin film surface roughness was improved compared with substrate surface roughness. This phenomenon of smoothing was also observed by de Assis et al. [41], *i.e.* the surface roughness reduction of deposited thin films depends on initial substrate surface roughness, on the growth method and the used material and is strongly correlated with the mobility of the sputtered adatoms. Another distinctive feature of this observation is the presence of defects (stacking faults) in the bulk of the Ir film. As a final point, repeating the same procedure as for the other films, 14 dislocations can be observed, which yields an average 2.68 nm of dislocation spacing. It should be mentioned that in this calculation the right hand side of the TEM image has been disregarded. Indeed, since the interface is poorly defined, the resulting FFT cannot be reliably analysed.

To conclude, the HR-TEM observations corroborate the film growth mechanism deduced from the XRD analysis of the residual strain: the film grows in a strain-relaxed state with the formation of geometrical misfit dislocations with an average spacing in the 10.5 – 10.9 range, in excellent agreement with the value derived by assuming a complete strain relaxation during growth (10.3 unit-cells). Thermal strain is subsequently stored within the film upon cooling down from the growth temperature, as a result of the film/substrate thermal expansion mismatch.

4. Conclusion

We report on the epitaxial growth of atomically smooth iridium films grown on single crystal substrates, *i.e.* MgO(001), (111), and (110), respectively, by DC-magnetron sputtering. Despite the fact that the growth of thin films with *fcc*-type structure generally is governed by the minimization of the surface energy, and thus the (111) crystalline direction is often preferred, hetero-epitaxial iridium thin films with (100), (111) and (110) crystallographic orientations is successfully achieved. The hetero-epitaxial relations between iridium thin films and MgO substrates can be attributed to the fact that the substrate acts as a crystallographic template for the growth of oriented Ir. It should be noted though that the surface energy still plays an important role, in particular by determining the overall crystalline quality of the films. In all cases, however, the iridium films exhibit flat topography with sub-nanometric surface roughness, making them a potential candidate for the template growth functional thin films.

Acknowledgements

This work was supported by a grant of the Romanian National Authority for Scientific Research and Innovation, CCCDI – UEFISCDI project number 61/2016 within PNCDI III, Core Program PN19-03 (contract no. 21 N/08.02.2019) and by the H2020 European project "MASTERS" within the M-ERA.NET call (http://www.unilim.fr/h2020_masters).

The authors gratefully acknowledge the help of Pierre CARLES and thank the CARMALIM team at the "*Centre Européen de la Céramique*" in Limoges, for their support in investigating the structure and morphology of the thin film samples.

References

[1] Y. Tolstova, S.T. Omelchenko, A.M. Shing, H.A. Atwater, "*Heteroepitaxial growth of Pt and Au thin films on MgO single crystals by bias-assisted sputtering*", Scientific Reports 6 (2016) 23232; https://doi.org/10.1038/srep23232

[2] M. Ohtake, S. Ouchi, F. Kirino, M. Futamoto, "*Structure and Magnetic Properties of CoPt, CoPd, FePt, and FePd Alloy Thin Films Formed on MgO(111) Substrates*", IEEE Transactions on Magnetics 48 (2012) 3595-3598; https://doi.org/10.1109/TMAG.2012.2198875

[3] T. Tanaka, M. Ohtake, F. Kirino, M. Futamoto, "*Microstructure of NiFe Epitaxial Thin Films Grown on MgO Single-Crystal Substrates*", IEEE Transactions on Magnetics 46 (2010) 345-348; https://doi.org/10.1109/TMAG.2009.2

[4] B. Borca, O. Frucharta, Ph. David, A. Rousseau, C. Meyer, "*Kinetic self-organization of trenched templates for the fabrication of versatile ferromagnetic nanowires*", Applied Physics Letters 90 (2007) 142507; https://doi.org/10.1063/1.2718510

[5] K. Wandelt (ed.), in: "*Surface and Interface Science, Volume 4*"; Wiley-VCH Verlag GmbH & Co. KGaA (2014), ISBN: 9783527411573; https://doi.org/10.1002/9783527680566

[6] H. Bensalah, I. Stenger, G. Sakr, J. Barjon, R. Bachelet, A. Tallaire, J. Achard, N. Vaissiere, K.H. Lee, S. Saada, J.C. Arnault; "*Mosaicity, dislocations and strain in heteroepitaxial diamond grown on iridium*"; Diamond and Related Materials 66 (2016) 188-195; https://doi.org/10.1016/j.diamond.2016.04.006

[7] M. Okada, S. Ogura, W.A. Diño, M. Wilde, K. Fukutani, T. Kasai; "*Reactivity of gold thin films grown on iridium: Hydrogen dissociation*"; Applied Catalysis A: General 291 (2005) 55-61; https://doi.org/10.1016/j.apcata.2005.02.040

[8] P. Kúš, A. Ostroverkh, K. Ševčíková, I. Khalakhan, R. Fiala, T. Skála, N. Tsud, V. Matolin; "*Magnetron sputtered Ir thin film on TiC-based support sublayer as low-loading anode*

catalyst for proton exchange membrane water electrolysis"; International Journal of Hydrogen Energy 41 (2016) 15124-15132; https://doi.org/10.1016/j.ijhydene.2016.06.248

[9] M. Wesselmark, B. Wickman, C. Lagergren, G. Lindbergh; "*The impact of iridium on the stability of platinum on carbon thin-film model electrodes*"; Electrochimica Acta 111 (2013) 152-159; https://doi.org/10.1016/j.electacta.2013.07.108

[10] J.S. Bessey, J.A. Roth; "*Sputtered iridium coatings for grazing incidence X-ray reflectance*"; Proceedings of SPIE 2011 (1994) 12-17; https://doi.org/10.1117/12.167202

[11] D.M. Broadway, J. Weimer, D. Gurgew, T. Lis, B.D. Ramsey, M. O'Dell, A. Gubarev, R. Bruni Ames; "*Achieving zero stress in iridium, chromium, and nickel thin films*"; Proceedings of SPIE 9510 (2015) 9510-9510-15; https://doi.org/10.1117/12.2180641

[12] E.A. Owen, E.L. Yates; "*Precision measurements of crystal parameters*"; Philosophical Magazine 15 (1933) 472-488; https://doi.org/10.1080/14786443309462199

[13] J.W. Arblaster; "*Crystallographic Properties of Iridium. Assessment of properties from absolute zero to the melting point*"; Platinum Metals Review 54 (2010) 93–102; https://doi.org/10.1595/147106710X493124

[14] H. Zhuang, A.J. Tkalych, E.A. Carter; "*Surface Energy as a Descriptor of Catalytic Activity*"; The Journal of Physical Chemistry C 120 (2016) 23698–23706; https://doi.org/10.1021/acs.jpcc.6b09687

[15] G.A. Somorjai, Y. Li; "*Impact of surface chemistry*"; PNAS 108 (2011) 917-924; https://doi.org/10.1073/pnas.1006669107

[16] E. Lang, K. Müller, K. Heinz, M.A. Van Hove, R.J. Koestner, G.A. Somorjai; "*LEED intensity analysis of the (1 × 5) reconstruction of Ir(100)*"; Surface Science 127 (1983) 347-365; https://doi.org/10.1016/0039-6028(83)90422-3

[17] M.A. Van Hove, R.J. Koestner, P.C. Stair, J.P. Bibérian, L.L. Kesmodel, I.Bartoš, G.A. Somorjai; "*The surface reconstructions of the (100) crystal faces of iridium, platinum and gold: I. Experimental observations and possible structural models*"; Surface Science 103 (1981) 189-217; https://doi.org/10.1016/0039-6028(81)90107-2

[18] J.T. Grant; "*A LEED study of the Ir(100) surface*"; Surface Science 18 (1969) 228; https://doi.org/10.1016/0039-6028(69)90167-8

[19] K. Christmann, G. Ertl; "*Interactions of CO and 0_2 with Ir(110) Surfaces*"; Zeitschrift für Naturforschung A 28a (1973) 1144-1148; https://doi.org/10.1515/zna-1973-0717

[20] R. Rai, T. Li, Z. Liang, M.K. Kim, A. Asthagiri, J.F. Weaver; "*Growth and termination of a rutile IrO_2(100) layer on Ir(111)*"; Surface Science 652 (2016) 213–221; http://dx.doi.org/10.1016/j.susc.2016.01.018

[21] A. Büttner, A.C. Probst, F. Emmerich, C. Damm, B. Rellinghaus, T. Döhring, M. Stollenwerk; "*Influence of sputtering pressure on microstructure and layer properties of iridium thin films*"; Thin Solid Films 662 (2018) 41–46; https://doi.org/10.1016/j.tsf.2018.06.056

[22] A. Ghalem, L. Huitema, A. Crunteanu, M. Rammal, L. Trupina, L. Nedelcu, M. G. Banciu, P. Dutheil, C. Constantinescu, P. Marchet, F. Dumas-Bouchiat, C. Champeaux; "*Electrical transport properties and modelling of electrostrictive resonance phenomena in $Ba_{2/3}Sr_{1/3}TiO_3$ thin films*"; Journal of Applied Physics 120 (2016) 184101; http://dx.doi.org/10.1063/1.4966942

[23] K. Nadaud, C. Borderon, R. Renoud, A. Ghalem, A. Crunteanu, L. Huitema, F. Dumas-Bouchiat, P. Marchet, C. Champeaux, H.W. Gundel; "*Domain wall motions in BST ferroelectric thin films in the microwave frequency range*"; Applied Physics Letters 109 (2016) 262902; https://doi.org/10.1063/1.4973451

[24] K. Nadaud, C. Borderon, R. Renoud, A. Ghalem, A. Crunteanu, L. Huitema, F. Dumas-Bouchiat, P. Marchet, C. Champeaux, H.W. Gundel; "*Effect of the incident power on permittivity, losses and tunability of BaSrTiO3 thin films in the microwave frequency range*"; Applied Physics Letters 110 (2017) 212902; https://doi.org/10.1063/1.4984089

[25] K. Nadaud, C. Borderon, R. Renoud, A. Ghalem, A. Crunteanu, L. Huitema, F. Dumas-Bouchiat, P. Marchet, C. Champeaux, H.W. Gundel; "*Diffuse phase transition of BST thin films in the microwave domain*"; Applied Physics Letters 112 (2018) 262901; https://doi.org/10.1063/1.5030485

[26] L.D. Madsen, R. Charavel, J. Birch, E.B. Svedberg, "*Assessment of MgO(1 0 0) and (1 1 1) substrate quality by X-ray diffraction*", Journal of Crystal Growth 209 (2000) 91-101; http://dx.doi.org/10.1016/s0022-0248(99)00533-3

[27] R. Suzuki, A. Kawaharazuka, Y. Horikoshi, "*Effect of the MgO substrate on the growth of GaN*", Journal of Crystal Growth 311 (2009) 2021-2024; http://dx.doi.org/10.1016/j.jcrysgro.2008.12.023

[28]. T. Ishikawa, Y. Abe, S. Shinkai, K. Sasaki; "*Epitaxial Ir Thin Film on (001) MgO Single Crystal Prepared by Sputtering*"; Japanese Journal of Applied Physics 42 (2003) 5747–5748; https://doi.org/10.1143/JJAP.42.5747

[29] T. Chen, X. Li, S. Zhang, X. Zhang; "*Comparative study of epitaxial growth of Pt and Ir electrode films grown on MgO-buffered Si(100) by PLD*"; Applied Physics A 80 (2005) 73-76; https://doi.org/10.1007/s00339-004-2978-2

[30] S. Gsell, M. Fischer, M. Schreck, B. Stritzker; "*Epitaxial films of metals from the platinum group (Ir, Rh, Pt and Ru) on YSZ- buffered Si(111)*"; Journal of Crystal Growth 311 (2009) 3731–3736; https://doi.org/10.1016/j.jcrysgro.2009.04.034

[31] L. Trupina, L. Nedelcu, C. Negrila, M. G. Banciu, L. Huitema, A. Crunteanu, M. Rammal,

A. Ghalem; "*Growth of highly textured iridium thin films and their stability at high temperature in oxygen atmosphere*"; Journal of Materials Science 51 (2016) 8711–8717; https://doi.org/10.1007/s10853-016-0131-1

[32] M.J. Mehl, D.A. Papaconstantopoulos; "*Applications of a tight-binding total-energy method for transition and noble metals: Elastic constants, vacancies, and surfaces of monatomic metals*"; Physical Review B 54 (1996) 4519-4530; https://doi.org/10.1103/PhysRevB.54.4519

[33] M. Grundmann, T. Bontgen, M. Lorenz; "*Occurrence of Rotation Domains in Heteroepitaxy*"; Physical Review Letters 105 (2010) 146102; https://doi.org/10.1103/PhysRevLett.105.146102

[34] J. Narayana, B.C. Larson; "*Domain epitaxy: A unified paradigm for thin film growth*"; Journal of Applied Physics 93 (2003) 278; https://doi.org/10.1063/1.1528301

[35] M. Birkholz; "*Thin Film Analysis by X-Ray Scattering*"; Wiley-VCH Verlag GmbH & Co. KGaA (2006); Online ISBN: 9783527607594; https://doi.org/10.1002/3527607595

[36] A. Boulle, R. Guinebretiere, O. Masson, R. Bachelet, F. Conchon, A. Dauger; "*Recent advances in high-resolution X-ray diffractometry applied to nanostructured oxide thin films: The case of yttria stabilized zirconia epitaxially grown on sapphire*"; Applied Surface Science 253 (2006) 95–105; https://doi.org/10.1016/j.apsusc.2006.05.086

[37] A. Boulle, S. Kilburger, P. Di Bin, E. Millon, C. Di Bin, R. Guinebretiere, A. Bessaudou; "*Role of nanostructure on the optical waveguiding properties of epitaxial $LiNbO_3$ films*"; Journal of Physics D: Applied Physics 42 (2009) 145403; https://doi.org/10.1088/0022-3727/42/14/145403

[38] A. Boulle; "*DxTools: processing large data files recorded with the Bruker D8 diffractometer*"; Journal of Applied Crystallography 50 (2017) 967–974; https://doi.org/10.1107/S1600576717005192

[39] A.S. Madhusudhan Rao, K. Narender; "*Studies on Thermophysical Properties of CaO and MgO by γ-Ray Attenuation*"; Journal of Thermodynamics (2014) 123478; http://dx.doi.org/10.1155/2014/123478

[40] J.L. Schroeder, A.S. Ingason, J. Rosén, J. Birch; "*Beware of poor-quality MgO substrates: A study of MgO substrate quality and its effect on thin film quality*"; Journal of Crystal Growth 420 (2015) 22-31; https://doi.org/10.1016/j.jcrysgro.2015.03.010

[41] T.A. de Assis, F.D.A. Aarao Reis; "Smoothening in thin-film deposition on rough substrates", Physical Review E 92 (2015) 052405; https://doi.org/10.1103/PhysRevE.92.052405

Tables & Figures (with captions)

hkl	*Thickness (nm)*	*Roughness (Å)*	*Distortions*	*Mosaicity (°)*	*In-plane strain (%)*	*Cell shrinkage (%)*	*Bi-axial Poisson ratio*
(100)	23	6.8	0.012	1.26	-0.353(9)	-3.586(5)	$2\,C_{12}/C_{11}$ (0.8441)
(111)	65	3.8	0	0.30	-0.36(1)	-3.10(2)	$(2C_{11} + 4C_{12} - 4C_{44}) / (C_{11} + 2C_{12} + 4C_{44})$ (0.5281)
(110)	20	10	0.011	1.30	-0.30(6)	-6	$(C_{11} + 3C_{12} - 2C_{44}) / (C_{11} + C_{12} + 2C_{44})$ (0.5965)

Table 1. Structural parameters obtained from the XRD analysis

a)

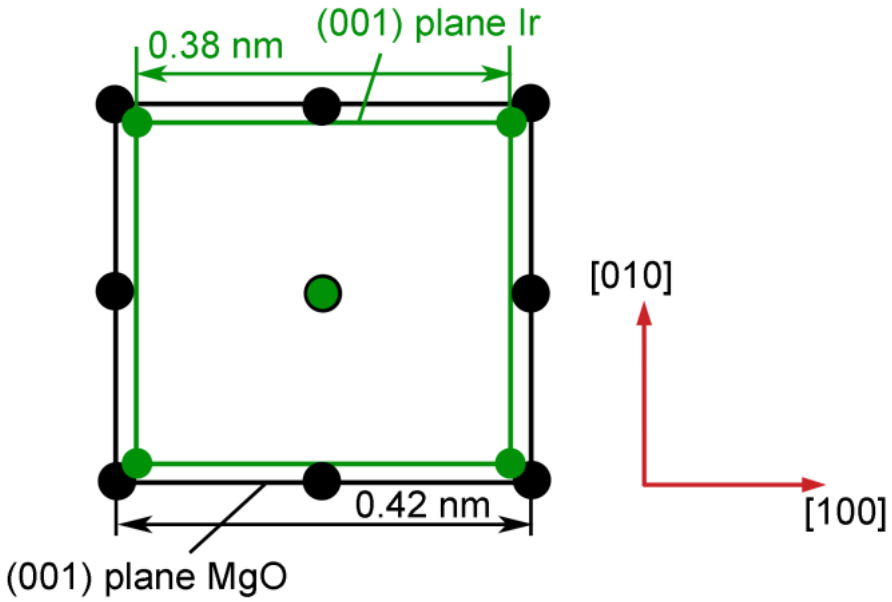
0.38 nm
(001) plane Ir
[010]
[100]
0.42 nm
(001) plane MgO

b)

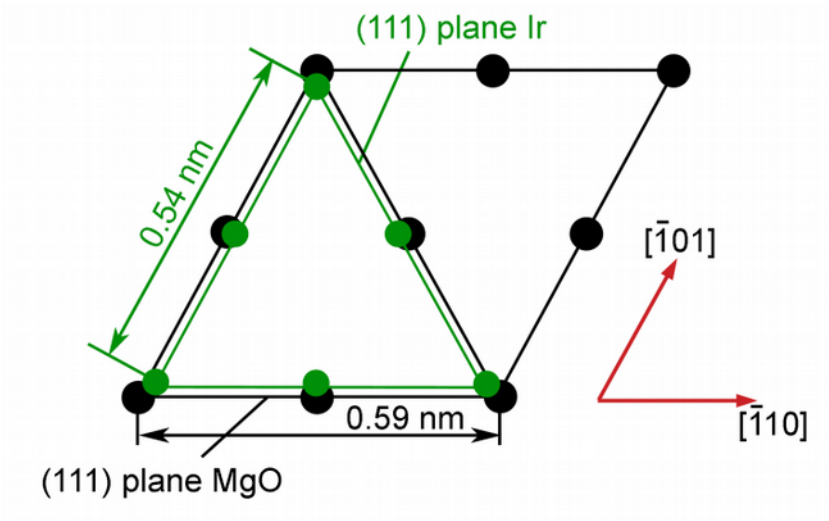
(111) plane Ir
0.54 nm
[$\bar{1}$01]
[$\bar{1}$10]
0.59 nm
(111) plane MgO

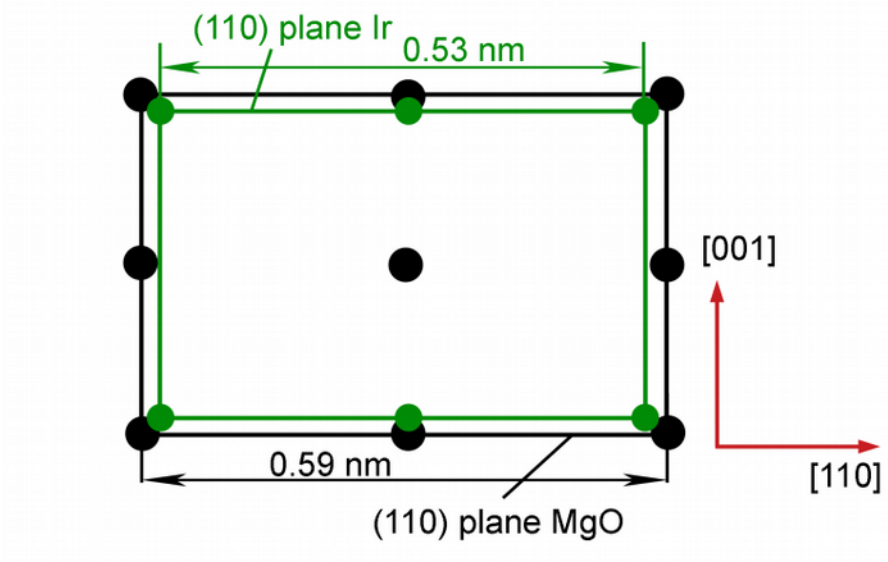

c)

Figure 1. Schematic of the possible hetero-epitaxial relations between (**a**) Ir(001) on MgO(001), (**b**) Ir(111) on MgO(111), and (**c**) Ir(110) on MgO(110) planes

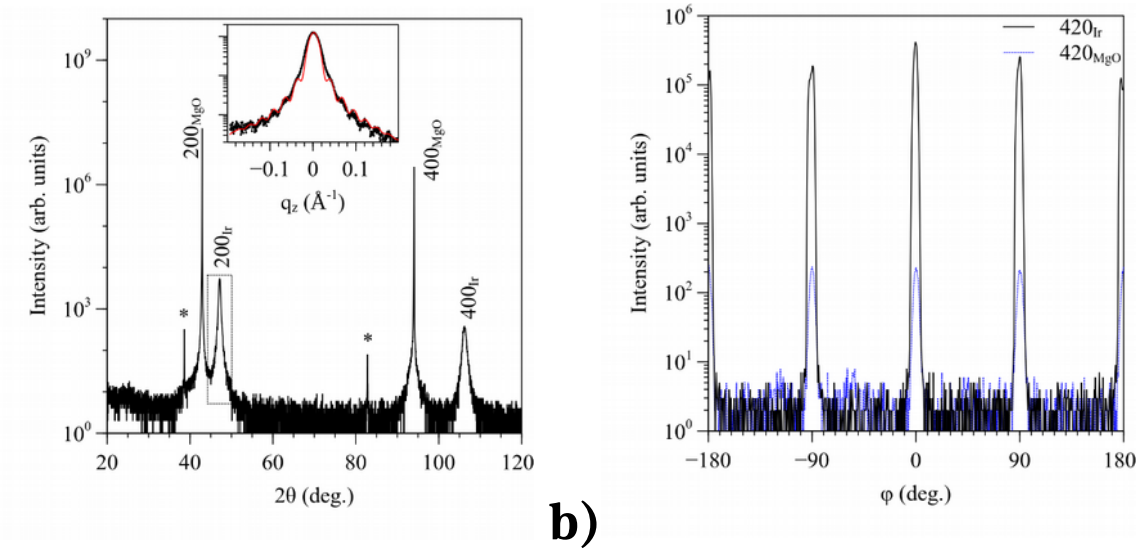

a) b)

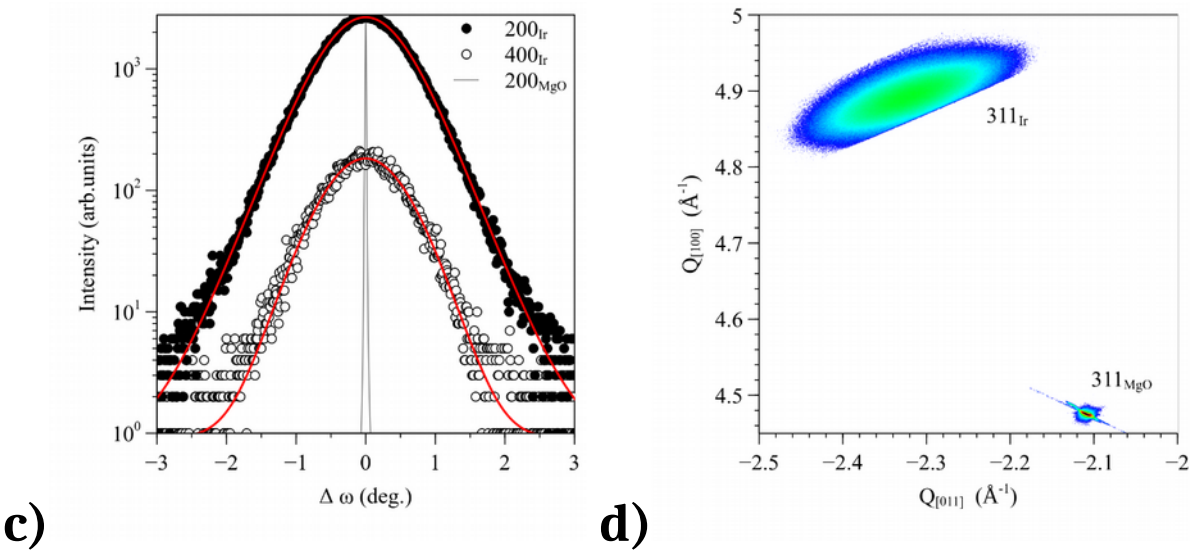

c) d)

Figure 2. X-ray θ-2θ diffraction scan patterns of (100) oriented iridium films deposited on (100)MgO substrate (**a**). Phi (Φ) scan plots of the (420) reflections of iridium and MgO(100 (**b**). Rocking curves recorded through the 200 and 400 reflection of Ir(100)/MgO(100) Circles: experimental data; red line: simulation. (**c**). Reciprocal space map of the 311 reflections of Ir and MgO (**d**)

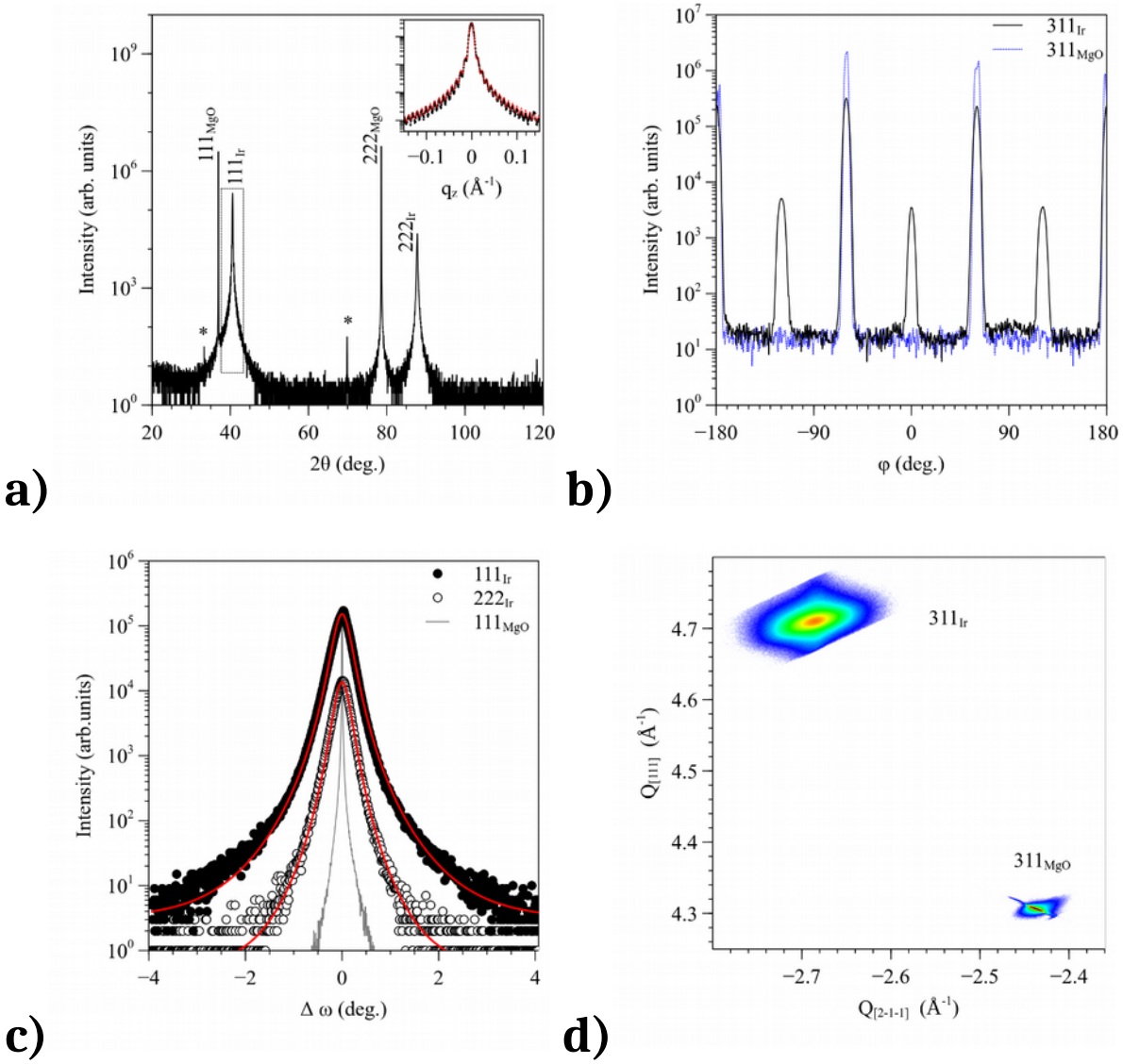

Figure 3. X-ray θ-2θ diffraction scan patterns of (111) oriented iridium films deposited on (111)MgO substrate (**a**). Phi (Φ) scan plots of the (311) reflections of iridium and MgO (**b**). Rocking curves recorded through the 111 and 222 reflection of Ir. Circles: experimental data; red line: simulation. (**c**). Reciprocal space map of the 311 reflections of Ir and MgO (**d**)

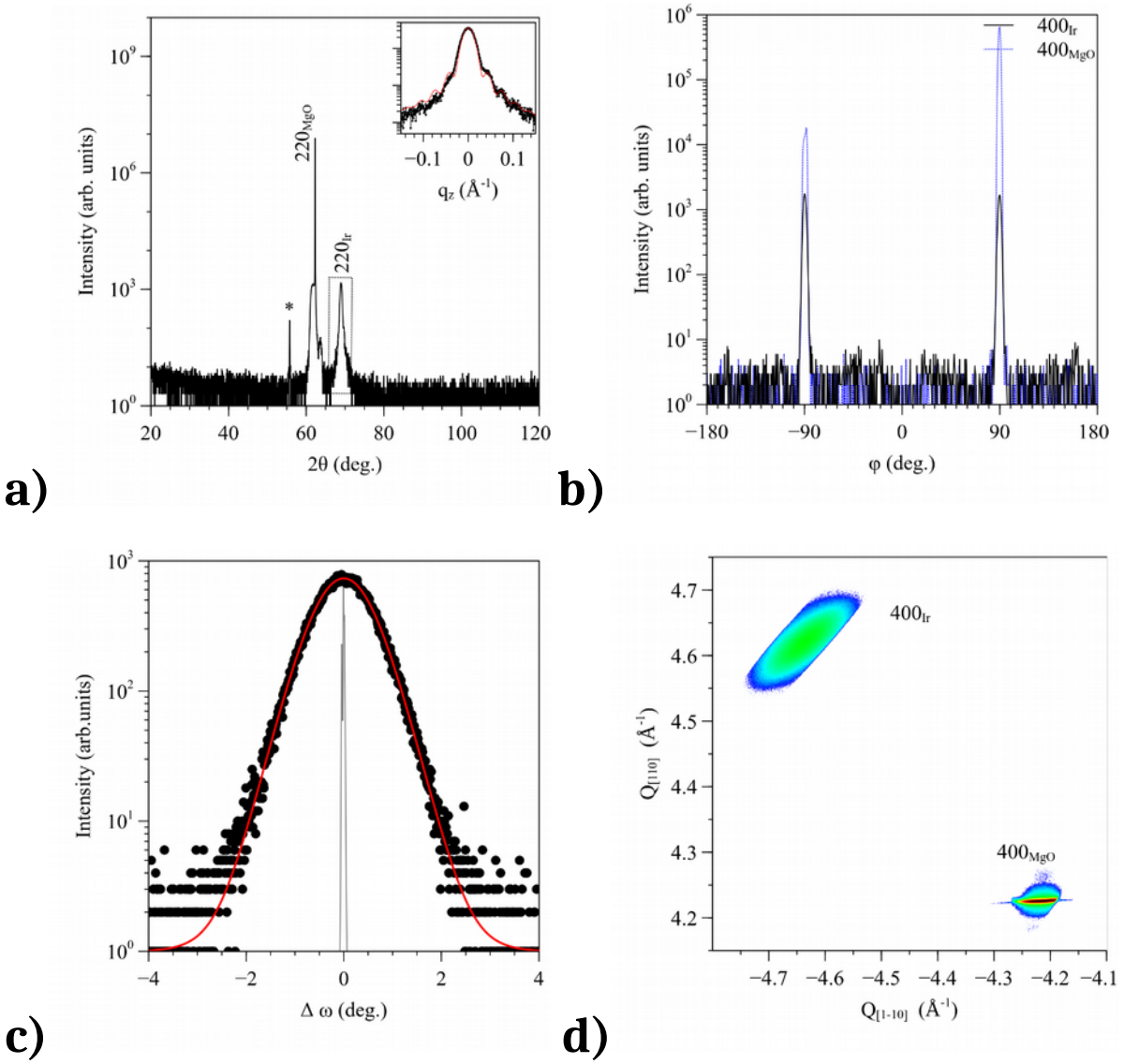

Figure 4. X-ray θ-2θ diffraction scan patterns of (110) oriented iridium films deposited on (111)MgO substrate (**a**). Phi (Φ) scan plots of the (400) reflections of iridium and MgO (**b**). Rocking curves recorded through the 220 reflection of iridium. Circles: experimental data; red line: simulation. (**c**). Reciprocal space map of the 400 reflections of iridium and MgO (**d**)

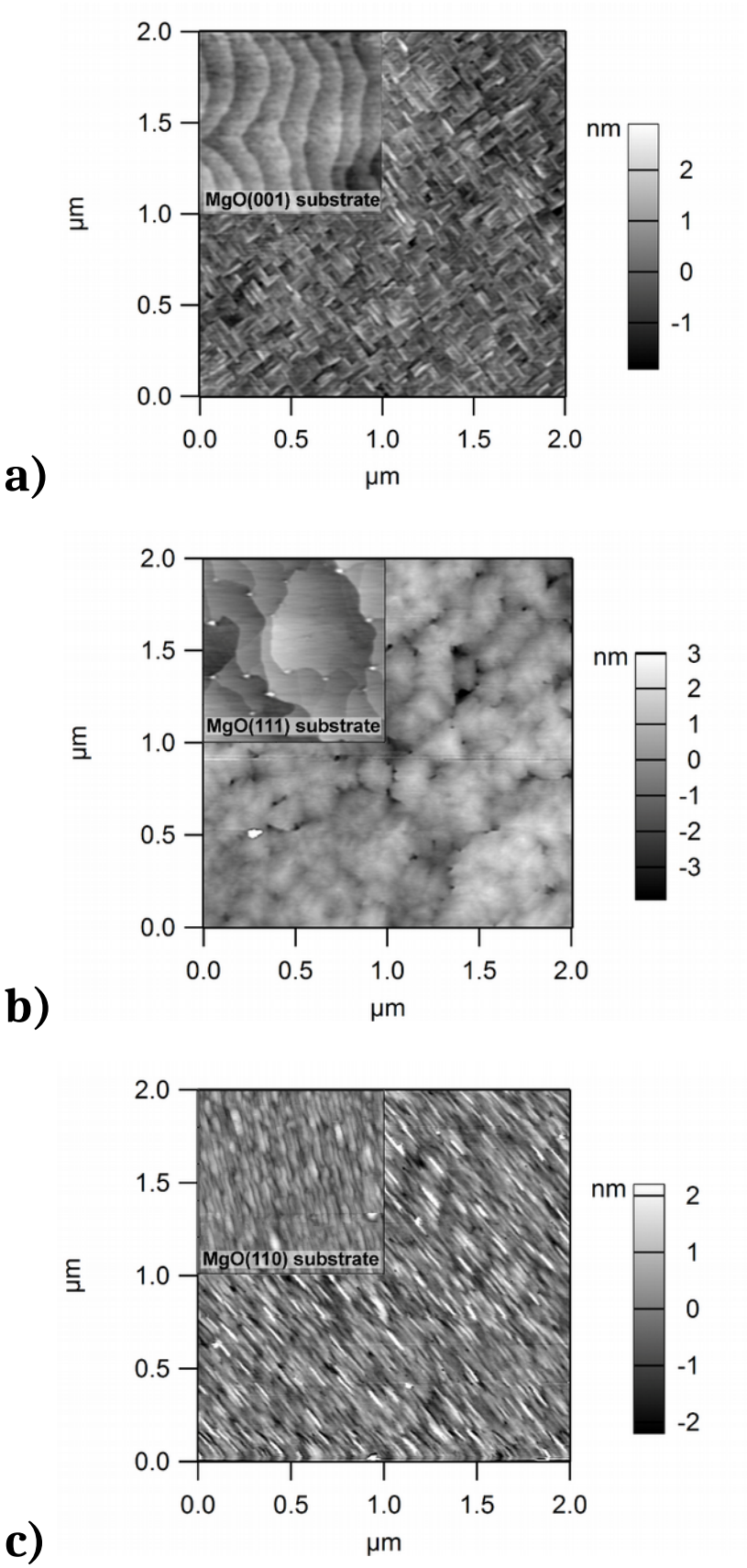

Figure 5. AFM images of (**a**) Ir(001), (**b**) Ir(111) and (**c**) Ir(110) grown on MgO-(001), (111) and (110), respectively. Inset images presents AFM images (1 µm x 1 µm) of substrates surface before film deposition

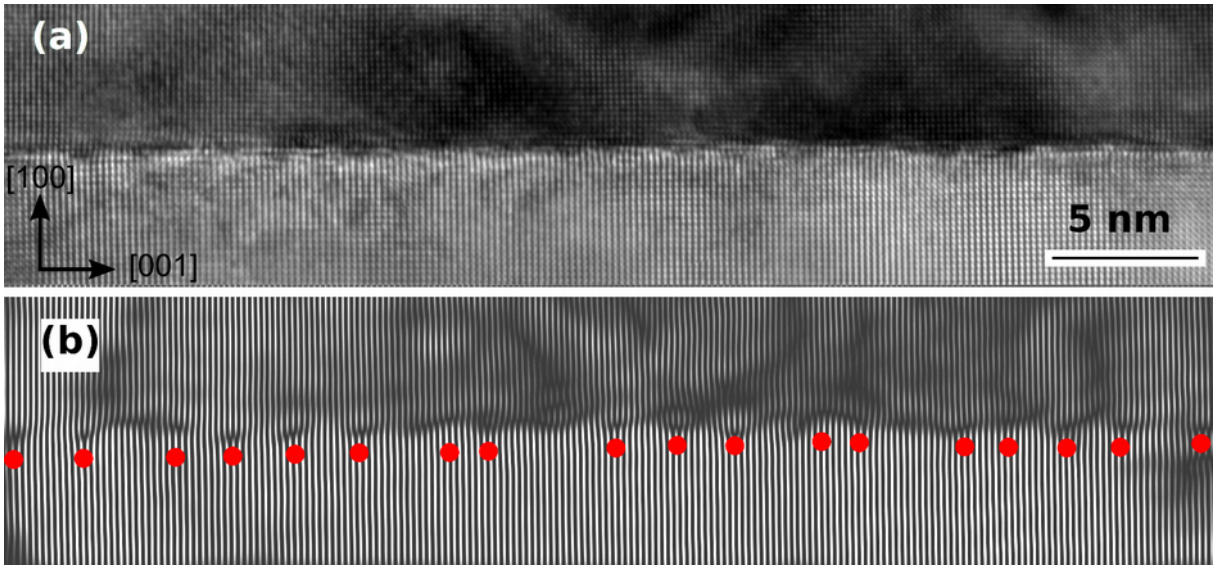

Figure 6. HR-TEM image of Ir(001) grown on MgO-(001) (**a**), and the corresponding filtered image (**b**)

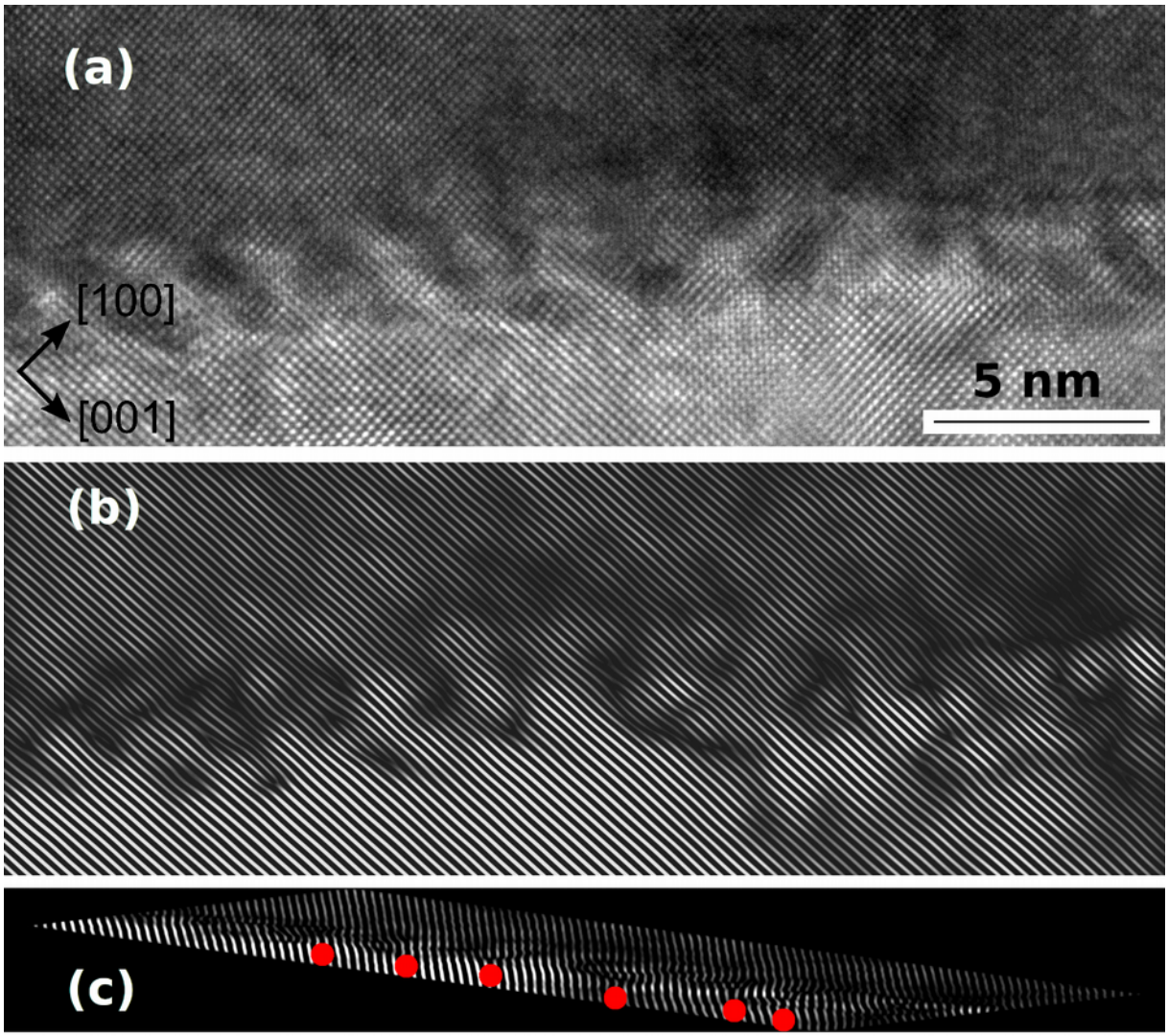

Figure 7. HR-TEM image of Ir(111) grown on MgO-(111) (**a**), and the corresponding filtered image (**b**); compressing the image along the selected {00l} planes allows one to resolve some misfit dislocations (**c**)

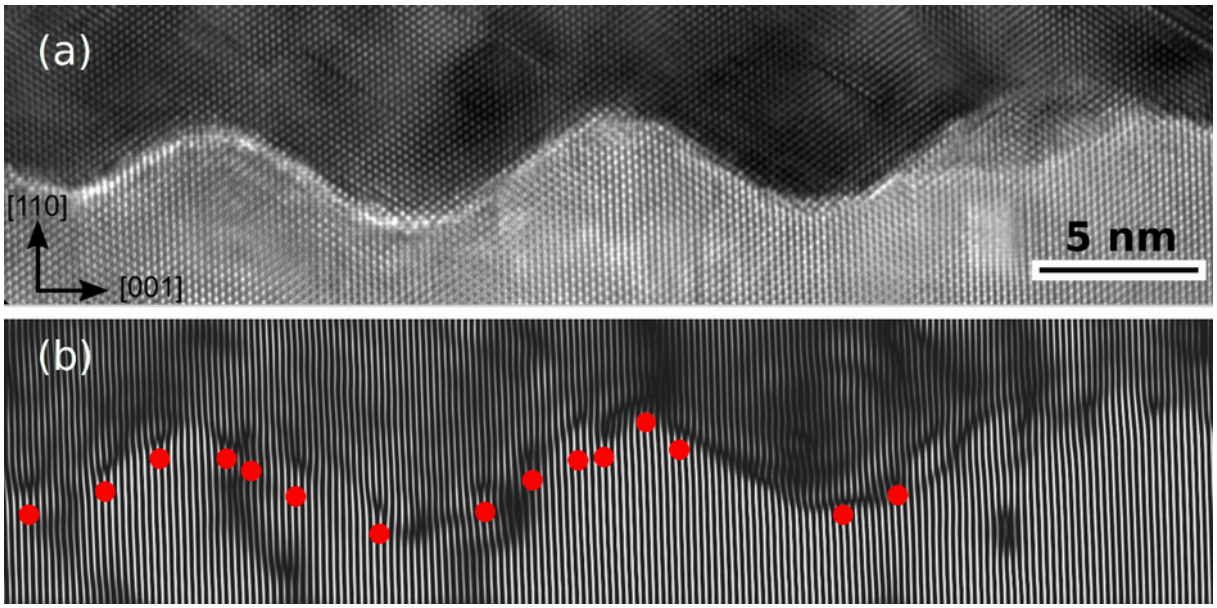

Figure 8. HR-TEM image of Ir(110) grown on MgO-(110) (**a**), and the corresponding filtered image (**b**), in which only those dislocations located at the interface have been taken into account; moreover, the right part of the figure without marked dislocations have been voluntarily disregarded since the interface is not clearly defined which leads to a very perturbed FFT filtered image

Texture and interface characterization of iridium thin films grown on MgO substrates with different orientations

[2]*Lucian TRUPINA*[1], *Liviu NEDELCU*[1], *Marian Gabriel BANCIU*[1],
Aurelian CRUNTEANU[2], *Laure HUITEMA*[2], [*]*Cătălin CONSTANTINESCU*[3], *Alexandre BOULLE*[3]

[1] *National Institute of Materials Physics,*
Bd. Atomistilor 405A, RO-077125 Magurele, Romania

[2] *XLIM - UMR 7252, CNRS, University of Limoges,*
123 av. Albert Thomas, F-87060 Limoges, France

[3] *IRCER - UMR 7315, CNRS, University of Limoges,*
12 rue Atlantis, F-87068 Limoges, France

Supplementary Material

In order to assess the quality and structure of the iridium thin films and the corresponding MgO substrates, TEM sample slides (~20 × 7 µm) are cut by FIB and then soldered to the TEM holders with Pt, as shown in *Figure 1* of this *Supplementary Material*. Samples are finally refined and thinned by FIB and with the help of a nanomanipulator are further transported and investigated. HR-TEM investigations of the iridium thin films *vs.* MgO substrates have been acquired at different magnifications and in several zones for all three crystalline orientations.

Selected area electron diffraction (SAED) patterns have been recorded from the film, the substrate as well as from the interfacial region for all films, as shown in *Figure 2* of this *Supplementary Material* (electron beam: 1 nm in diameter).

[2] Electronic mail: *lucian.trupina@infim.ro*, *catalin.constantinescu@unilim.fr*

a)

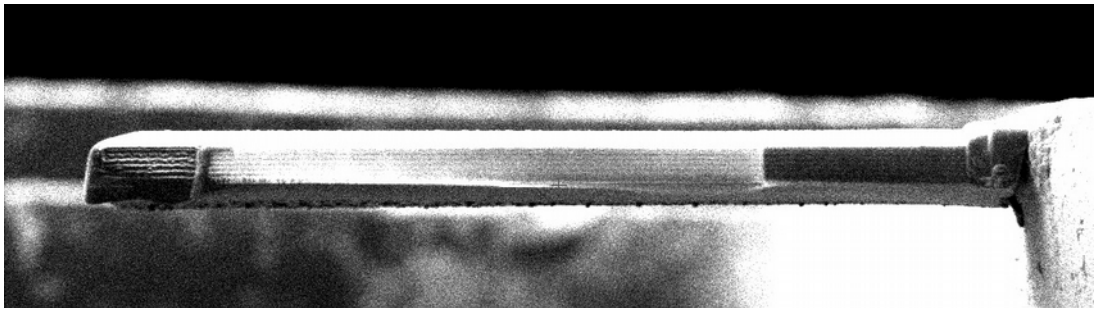

b)

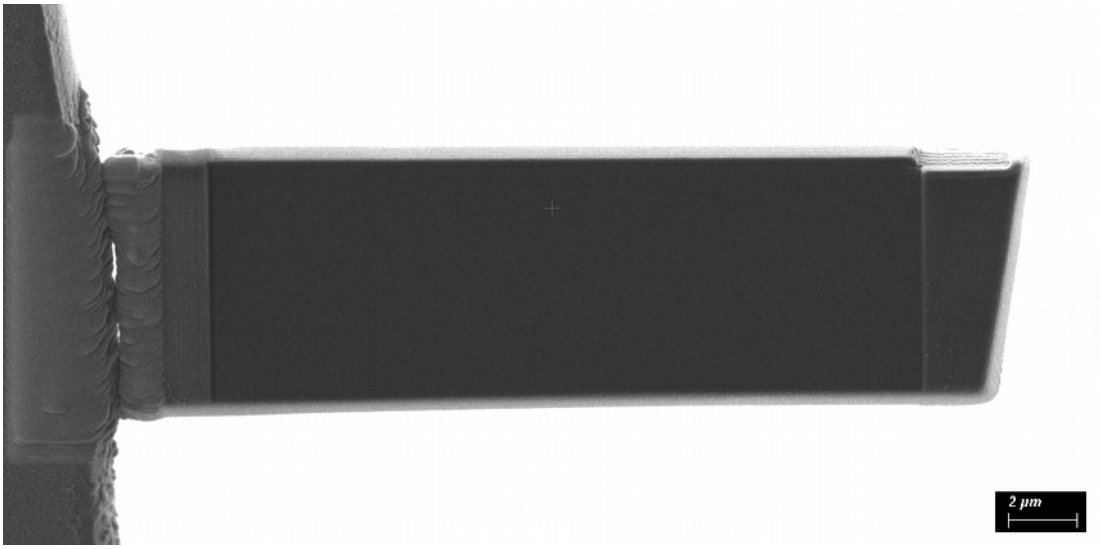

Figure 1. SEM images of a FIB cut slide soldered to the TEM holder: top **(a)** and side view **(b)**

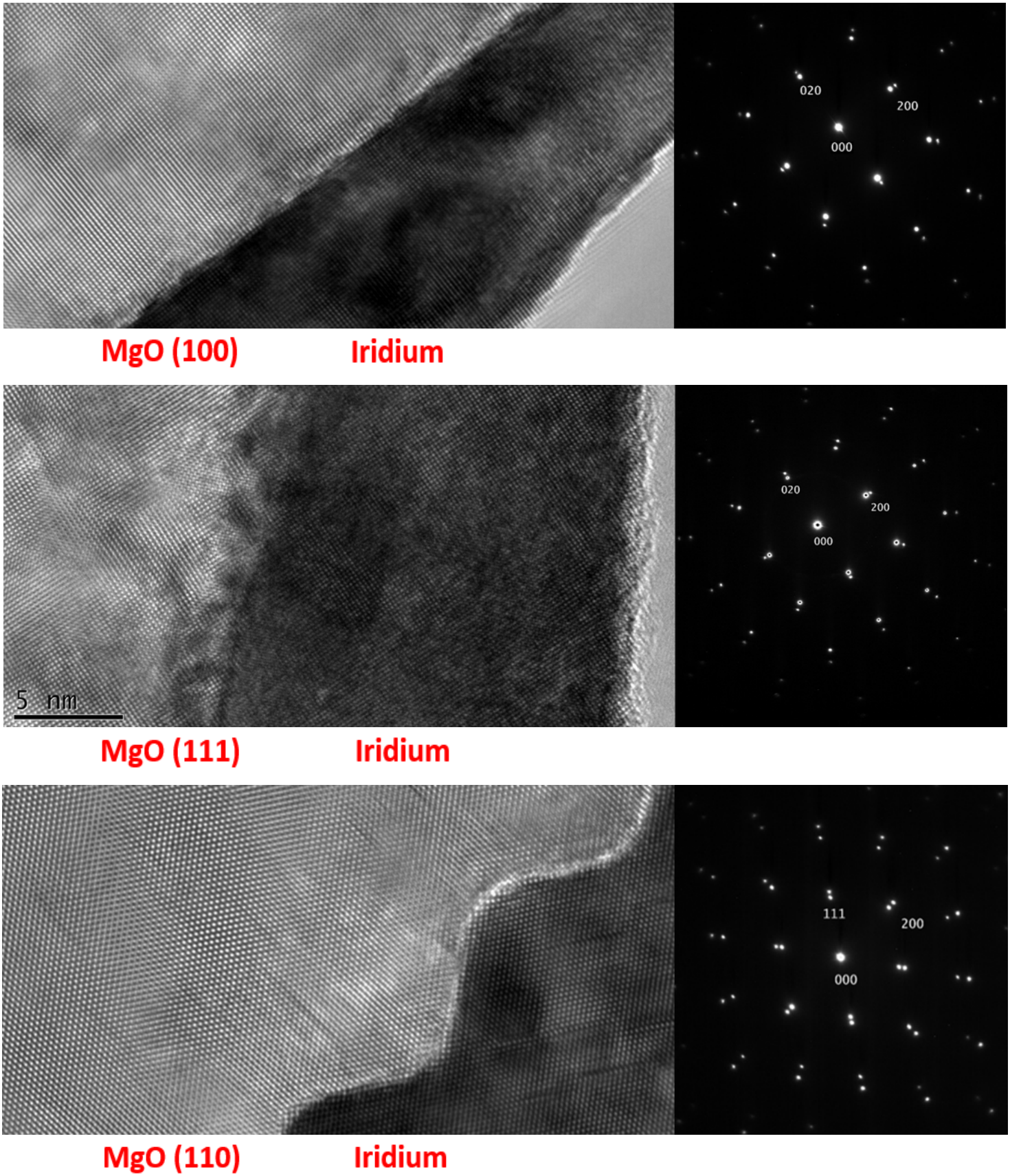

Figure 2. SAED diffraction patterns on the corresponding Ir/MgO samples with various crystallographic orientations, *i.e.* (100), (111), (110); images have identical scale bar (5 nm).